COMP4801 Final Year Project

Final Report: Enhanced Channel Charting Through CSI-based Distance Tracking Without Extra Cost

香 港 大 學

THE UNIVERSITY OF HONG KONG

Aveline Xiaoyuan Han

Date of Submission: 21st Apr 2025

Acknowledgment

Firstly, I would like to extend my sincere gratitude to Professor Wu Chenshu, my supervisor, for allowing me to make all kinds of mistakes along the journey. He gave me the freedom to explore this field, while consistently offering insightful suggestions and patiently answering all of my questions, no matter how trivial they may have seemed. It has been a great honor to work with him during my undergraduate studies.

I would also like to express my heartfelt thanks to Mr. WeiYing Hou (soon to be Dr. Hou), for his detailed guidance and constructive feedback—not only on this project, but throughout my entire research journey. He is a role model in the field of research, and I aspire to follow in his footsteps.

I am deeply grateful to Mr. Sheng Lyu, Mr. Xie Zhang, and Mr. Songlin Huang for their continuous support and assistance on this project. I also wish to thank all members of the HKU AIoT Lab for their encouragement and collaboration.

Lastly, I would like to thank my parents for their unwavering emotional (and financial) support. Their encouragement and belief in me have been a constant source of strength, helping me overcome the many challenges throughout my undergraduate life.

Gu yu sui yu, zu huo you suo wen.
Though I began with limited understanding, I am fortunate to have come this far, guided and uplifted by those who walked ahead of me.

Abstract

This research advances Channel Charting by introducing a novel distance-based approach that leverages Time Reversal Resonating Strength (TRRS) to create accurate spatial representations of indoor environments without requiring explicit position information. While traditional indoor localization methods face limitations due to labor-intensive site surveys and environmental sensitivity, and existing Channel Charting approaches often struggle to capture accurate spatial relationships without additional hardware or motion constraints, this work demonstrates that TRRS can serve as a reliable proxy for physical distance between wireless measurements. The methodology introduces a three-stage approach: first, computing pair-wise moving distances through TRRS analysis of Channel State Information (CSI) measurements; second, constructing a comprehensive dissimilarity matrix that combines TRRS-derived distances with cosine-based metrics; and third, employing deep learning-based manifold learning for dimensional reduction. Evaluation on the DICHASUS dataset, encompassing both line-of-sight and non-line-of-sight scenarios, demonstrates the effectiveness of distance estimation using TRRS, achieving a Mean Squared Error of 0.1691 m and Mean Absolute Error of 0.2932 m. The resulting channel charts show superior preservation of both local and global spatial relationships, outperforming baseline methods across all metrics including Continuity, Trustworthiness, and Kruskal's Stress scores. These results establish TRRS-based distance estimation as a fundamental advancement in Channel Charting, enabling robust indoor spatial awareness without specialized hardware or position labels.

Table of Contents

List of Figures

List of Abbreviations

- ADP: Angel-Delay Profile
- AoA: Angle-of-Arrival
- AP: Access Point
- CIR: Channel Impulse Response
- CMD: Correlation Matrix Distance
- CSI: Channel State Information
- CT: Continuity
- FM: Frequency Modulation
- GPS: Global Positioning System
- IMU: Inertial Measurement Unit
- IoT: Internet of Things
- KS: Kruskal's Stress
- LLE: Locally Linear Embedding
- LoS: Line-of-Sight
- MAE: Mean Absolute Error
- MDS: Multidimensional Scaling
- mmWave: millimeter Wave
- MSE: Mean Squared Error
- NLoS: None-Line-of-Sight
- OFDM: Orthogonal Frequency Division Multiplexing
- PCA: Principal Component Analysis
- PDR: Pedestrian Dead Reckoning
- RFID: Radio Frequency Identification

- RP: Reference Point
- RSS: Received Signal Strength
- RSSI: Received Signal Strength Indicator
- TDoA: Time-Difference-of-Arrival
- ToF: Time of Flight
- TRRE: Time Reversal Resonating Effect
- TRRS: Time Reversal Resonating Strength
- TW: Trustworthiness
- UE: User Equipment

1 Introduction

Channel Charting has emerged as a transformative technology in wireless communications, representing a paradigm shift in location-aware services and network optimization. This innovative technique has garnered significant attention in recent years, owing to its broad applicability in downstream tasks such as indoor user localization [1], radio resource management [2], and millimeter wave (mmWave) beam management [3]. Beyond these primary applications, Channel Charting shows promising potential in emerging fields such as autonomous navigation, smart building management, context-aware service delivery, and next-generation wireless networks. The technology's ability to create meaningful spatial representations without explicit position information makes it particularly valuable for privacy-preserving applications and scenarios where traditional positioning systems are impractical or unreliable.

The significance of Channel Charting extends far beyond its immediate applications. In the era of 5G and beyond, wireless networks are expected to support an unprecedented density of connected devices, with demands for ultra-reliable low-latency communications (URLLC) and enhanced mobile broadband (eMBB) services [4]. These requirements necessitate sophisticated spatial awareness and resource management capabilities, where Channel Charting can play a crucial role. Furthermore, as Internet of Things (IoT) deployments continue to expand, the need for efficient, scalable, and privacy-preserving localization solutions becomes increasingly critical [5]. Channel Charting addresses these challenges by providing a framework that can adapt to dynamic environments while maintaining user privacy and requiring minimal infrastructure modifications.

Specifically, this research focuses on leveraging the rich information embedded within widely available Wi-Fi signals to enable Channel Charting and related localization tasks. Indoor localization has traditionally relied on various radio-based techniques to estimate device positions by analyzing transmitted and received radio frequency signals [6]. Conventional approaches, such as trilateration and multilateration based on time-of-flight (ToF) [7] or time-difference-of-arrival (TDoA) [8], can achieve high accuracy under ideal conditions. However, these methods require an unobstructed Line-of-Sight (LoS) path between transmitter and receiver, with minimal reflection, scattering, diffraction, or obstruction [9]. In practical indoor environments, where such assumptions are frequently violated due to complex multipath propagation, localization accuracy degrades significantly [10].

Wi-Fi fingerprinting has emerged as a promising alternative that can function effectively even in complex multipath environments, avoiding the strict requirements of traditional methods. However, this approach faces its own set of challenges. The technique requires an extensive site survey process involving manual collection and labeling of signal data at numerous reference points [11]. Furthermore, fingerprinting performance is inherently sensitive to environmental dynamics. Since the technique relies on Channel State Information (CSI), which characterizes signal propagation between transmitter and receiver, any changes in the surrounding environment can significantly alter the radio fingerprint and compromise system reliability [12]. These fundamental limitations have motivated the development of more robust and adaptive solutions, particularly the Channel Charting approach presented in this work.

The fundamental challenge in indoor localization lies in creating accurate spatial representations of radio environments without relying on labor-intensive site surveys or maintaining strict line-of-sight conditions. Traditional approaches either require extensive manual data collection or fail in complex multipath environments, while existing fingerprinting methods remain vulnerable to environmental changes. This creates a pressing need for a solution that can automatically learn and adapt to indoor spatial relationships while maintaining reliability and scalability.

To address these challenges, this work explores Channel Charting as a promising self-supervised learning framework. Channel Charting offers a novel approach by learning spatial relationships directly from CSI measurements, eliminating the need for explicit position labels or extensive calibration. In wireless systems, while CSI exists in a complex, high-dimensional space shaped by multipath propagation, the actual physical movement of user equipment (UE) occurs in a lower-dimensional spatial domain (2D or 3D) [13]. This dimensional disparity presents an opportunity to uncover the latent spatial structure through manifold learning techniques.

Channel Charting provides several key advantages for indoor localization. The framework preserves user privacy by working with relative spatial relationships rather than explicit tracking. It operates independently of additional hardware beyond existing wireless infrastructure. The self-supervised learning approach enables automatic adaptation to environmental changes without manual recalibration. The system demonstrates excellent scalability, accommodating increasing numbers of users and devices without significant performance degradation. Once trained, the framework provides rapid position estimates with minimal computational overhead.

Channel Charting comprises two main stages. First, a dissimilarity matrix is computed using pairwise comparisons of CSI samples in the high-dimensional space, based on a chosen dissimilarity metric. Second, the low-dimensional embedding is obtained using either classical manifold learning techniques such as Isomap [14] and Sammon's Mapping [13], or deep learning-based approaches [15, 16, 17, 18]. Prior work has explored dissimilarity measures derived from CSI [14], side information [13], or a combination of both [10].

However, existing Channel Charting implementations face several critical challenges. Current approaches often rely on restrictive assumptions about user motion or require additional hardware for accurate distance estimation. Moreover, the selection of appropriate dissimilarity metrics that reliably capture spatial relationships remains an open problem. This work addresses these limitations by introducing Time Reversal Resonating Strength (TRRS) as a fundamental metric for constructing reliable spatial relationships between wireless channel measurements. The proposed approach leverages the unique properties of TRRS to estimate relative distances between CSI measurements without requiring motion constraints or auxiliary sensors, while maintaining robustness to environmental changes.

This research presents several significant contributions to the field of Channel Charting. First, it introduces a novel TRRS-based moving distance dissimilarity metric that enables accurate estimation of spatial relationships without requiring motion constraints or additional hardware. Second, the work develops a comprehensive methodology for constructing and enhancing dissimilarity matrices through the fusion of TRRS-derived distances and cosine-based metrics. Third, it implements and evaluates sophisticated deep learning architectures, including both Siamese and Triplet networks, for effective dimensional reduction. The experimental results demonstrate superior performance in both moving distance estimation (achieving MSE of 0.1691 m and MAE of 0.2932 m) and channel chart generation, as evidenced by improved Continuity, Trustworthiness, and Kruskal's Stress metrics compared to baseline methods. These achievements establish TRRS-based moving distance as a powerful tool for enhancing the accuracy and reliability of Channel Charting applications while maintaining the framework's inherent advantages of privacy preservation and infrastructure independence.

The remainder of this report is structured as follows: Section 2 introduces the preliminary concepts and background. Section 3 offers a comprehensive review of related work in the area of Channel Charting. Section 4 details the proposed methodology and system design. Section 5 presents and analyzes the experimental results. Finally, Section 6 summarizes the findings and discusses potential directions for future research.

2 Preliminary

This section provides an overview of the fundamental concepts essential for understanding wireless indoor localization, Channel State Information (CSI), and Channel Charting. It begins by introducing the basics of wireless channels and their characteristics, followed by a discussion of traditional localization methods and their limitations. The concept of Channel Charting is then introduced, along with the Time Reversal Resonating Effect and Manifold Learning, which are leveraged in this research.

2.1 What is "Channel"

Definition. A wireless channel represents the physical medium through which electromagnetic waves propagate between a transmitter and receiver. In indoor environments, the channel characteristics are fundamentally shaped by complex multipath phenomena, where transmitted signals reach the receiver through multiple paths due to interactions with the physical environment. These interactions primarily include reflection from walls and furniture, diffraction around corners, and scattering from various surfaces [12]. Figure 1 illustrates a typical multipath propagation scenario, showing the relationship between transmitted signals, received signals, and their corresponding channel responses.

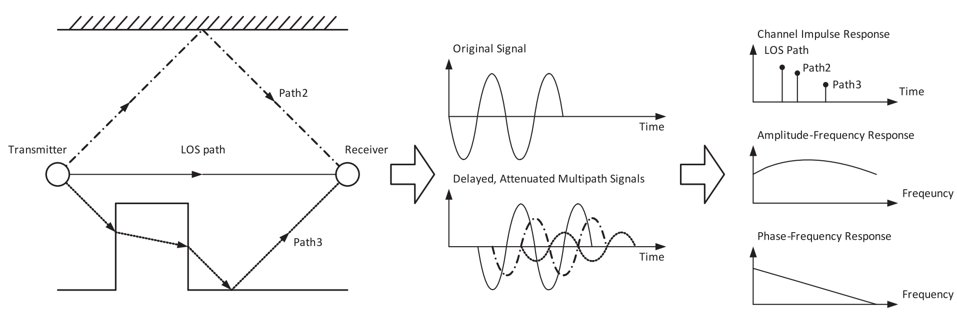

Figure 1: Illustration of multipath propagation, received signals, and channel responses in an indoor environment [12]

Channel Measurements. In wireless communications, the received signal Y is related to the transmitted signal X through the channel matrix H:

$$Y = HX,$$

where H represents the Channel State Information (CSI). In a multipath environment, the received signal Y is the superposition of multiple signal components, each following a different propagation path. Each path contributes a differently delayed, attenuated, and phase-shifted version of the transmitted signal. For N distinct paths, the received baseband signal voltage can be expressed as:

$$Y = \sum_{i=1}^{N} A_i X e^{-j\theta_i},$$

where A_i and θ_i denote the attenuation and phase shift of the i^{th} path respectively.

Channel Estimation. The wireless channel can be characterized in two complementary domains: time and frequency. In the time domain, the Channel Impulse Response (CIR), denoted as $h(t)$, describes how the channel responds to an impulse signal. The CIR captures the temporal distribution of multipath components, providing information about the delays and amplitudes of different signal paths:

$$h(t) = \sum_{i=1}^{L} \alpha_i \delta(t - \tau_i),$$

where α_i and τ_i represent the complex amplitude and delay of the i^{th} path respectively, and L is the total number of paths.

The frequency domain representation, known as the Channel Frequency Response (CFR) or CSI, is obtained through the Fourier transform of the CIR:

$$H(f) = \mathcal{F}\{h(t)\} = \sum_{i=1}^{L} \alpha_i e^{-j2\pi f \tau_i}$$

Channel State Information. In modern Wi-Fi systems employing Orthogonal Frequency Division Multiplexing (OFDM), CSI is measured across multiple subcarriers. For a system with N subcarriers, the CSI is represented as a vector:

$$\mathbf{H} = [H[0], H[1], \ldots, H[N-1]],$$

where each $H[k] = |H(k)|e^{j\angle H(k)}$ represents the complex channel gain at subcarrier k. The magnitude $|H(k)|$ indicates the attenuation, while the phase $\angle H(k)$ captures the phase shift introduced by the channel at that frequency.

In practice, CSI can be decomposed into static and dynamic components:

$$H(f,t) = H_s(f,t) + H_d(f,t),$$

where $H_s(f,t)$ represents the contribution from static paths (including Line-of-Sight and reflections from stationary objects), and $H_d(f,t)$ captures the effects of dynamic paths. For a moving receiver at position $d(t)$, the dynamic component can be expressed as:

$$H_d(f,t) = A(f,t)e^{-j2\pi\frac{d(t)}{\lambda}},$$

where $A(f,t)$ represents the amplitude and λ is the wavelength.

The Received Signal Strength Indicator (RSSI), commonly used in wireless systems, provides a coarse measurement of signal strength by computing the total received power across all subcarriers:

$$RSSI = 10\log_2(\frac{1}{N}\sum_{k=0}^{N-1}|H[k]|^2)$$

While RSSI is easily accessible, it discards the rich phase information and frequency-selective characteristics captured by CSI, making it less suitable for fine-grained localization applications.

2.2 What is "Charting"

Definition. Channel Charting represents a self-supervised learning approach that creates a low-dimensional representation of wireless channel measurements, preserving the spatial relationships between transmitter locations. This technique transforms high-dimensional Channel State Information (CSI) into a "chart" where the relative distances between points reflect the physical distances between the corresponding measurement locations. The fundamental principles and theoretical framework of Channel Charting were first established by [13].

Channel Feature Engineering. The first step in Channel Charting involves transforming the raw CSI measurements $H(f,t)$ into suitable feature vectors $\mathbf{f}$. These features are designed to capture the large-scale fading characteristics of the wireless channel while being robust to small-scale fading effects. For a system with N subcarriers and multiple measurement time instances, the feature extraction process can be represented as:

$$\mathbf{f} = \Phi(H[0], H[1], \ldots, H[N-1]),$$

where $\Phi(\cdot)$ denotes the feature extraction function that processes the complex channel gains across all subcarriers.

Charting Function. The core of Channel Charting lies in learning a mapping function C that transforms these channel features into points in a lower-dimensional space while preserving spatial relationships:

$$C : \mathbf{f} \mapsto \mathbf{z} \in \mathbb{R}^d,$$

where $\mathbf{z}$ represents the position in the channel chart and d (typically 2 or 3) is the dimension of the chart space. This mapping should satisfy two key properties:

- **Continuity:** Similar channel features $\mathbf{f}_i$ and $\mathbf{f}_j$ should map to nearby points $\mathbf{z}_i$ and $\mathbf{z}_j$ in the chart
- **Distance Preservation:** The relative distances between points in the chart should reflect the physical distances between the corresponding measurement locations

Learning Objective. The charting function C is learned by minimizing a loss function that encourages the preservation of spatial relationships:

$$\mathcal{L}(C) = \sum_{i,j} L(d(\mathbf{f}_i, \mathbf{f}_j), \|\mathbf{z}_i - \mathbf{z}_j\|),$$

where $d(\cdot, \cdot)$ measures the dissimilarity between channel features, and $\|\mathbf{z}_i - \mathbf{z}_j\|$ represents the Euclidean distance in the chart space. This optimization is performed without requiring any ground truth position information, making it a truly self-supervised learning approach.

The effectiveness of Channel Charting is illustrated in Figure 2, where the ground truth positions (Figure 2a) are compared with their corresponding representations in the learned channel chart (Figure 2b). The preservation of the ”VIP” curve structure and the smooth color gradients in the channel chart demonstrate the successful maintenance of local geometric relationships. This learned representation provides a consistent reference frame for location-dependent applications, enabling various downstream tasks such as localization, tracking, and mobility management.

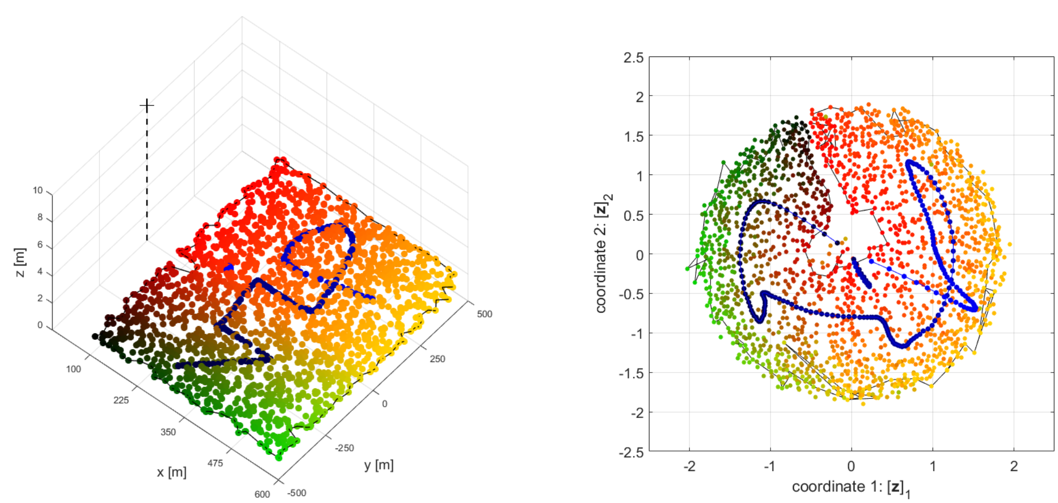

(a) 3D view on the considered system scenario

(b) Learned Channel Chart

Figure 2: Illustration of Channel Charting [13]. (a) Measured CSI from 2048 distinct gradient colored points in space; (b) Channel chart obtained from channel features in an unsupervised manner.

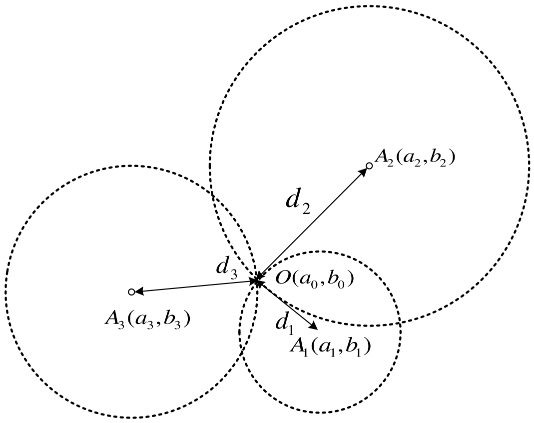

(a) Model-Based [19]

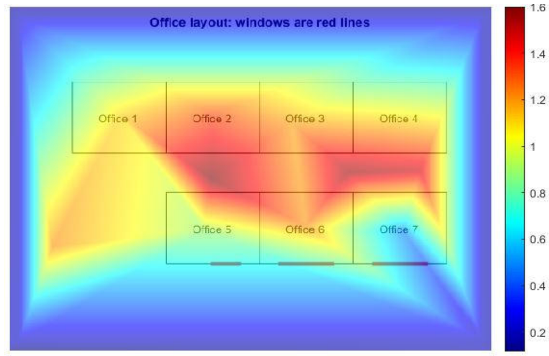

(b) Fingerprinting-Based

Figure 3: Traditional Localization Methods

2.3 Indoor Localization

As stated in both Section 1 and 2, one vital potential application of Channel Charting is Indoor user Localization. In today's modern contexts characterized by the proliferation of indoor environments such as airports, shopping malls, and university buildings, indoor localization is of utmost importance. Indoor localization pertains to the precise determination of a device's or user's position within enclosed spaces. This capability holds substantial potential for applications such as indoor guiding navigation, building management, surveillance and industrial operations [20]. Despite over three decades of dedicated research in indoor localization, practical solutions have yet to be realized. Two main categories of Wi-Fi localization methods designed for indoor scenarios are (1) Model-Based Localization (Figure 3a) and (2) Fingerprinting-Based Localization (Figure 3b).

2.3.1 Model-Based Localization

Model-based approaches establish mathematical relationships between signal characteristics and physical positions through geometric principles [21]. These methods can be categorized based on the signal parameters they utilize. Time-based methods employ signal propagation time measurements through techniques such as Time of Flight (ToF) [7] or Time Difference of Arrival (TDoA) [8]. While these methods can achieve high accuracy under ideal conditions, they require precise time synchronization and unobstructed Line-of-Sight (LoS) paths.

A simpler approach utilizes Received Signal Strength (RSS) measurements [22], converting signal strength into distance estimates through path loss models. Despite their implementation simplicity, these methods often suffer from significant errors due to multipath effects and environmental dynamics. More sophisticated techniques measure the Angle of Arrival (AoA) [23] or Angle of Departure (AoD) using antenna arrays. Although these angle-based methods can provide high accuracy, they require specialized hardware and are particularly sensitive to Non-Line-of-Sight (NLoS) conditions.

2.3.2 Fingerprinting-Based Localization Technique.

Fingerprinting-Based methods involve creating a Radio Map (or fingerprint database) of signal strength or other signal characteristics across various points within an indoor environment[21]. These signal "fingerprints" serve as Reference Points (RP) for determining the location of a device or user based on the similarity of the current signal readings to those stored in the Radio Map. Many previous researchers have delved into the Wi-Fi fingerprinting method, and it works in two phases (See Figure 4 below). First is the offline phase, also called site survey, during which researchers collect the Wi-Fi signal channel, namely, the Wi-Fi fingerprints from surrounding Access Points (APs) at every RP. By relating the Wi-Fi signal with the collected location, a fingerprint database is constructed. Next in the online phase, this fingerprint database is queried with a real-time Wi-Fi signal fingerprint sent by a user. Consequently, the localization algorithm will find the best match of this fingerprint in the database and return the corresponding location as the user's location [24].

Despite the fact that Wi-Fi fingerprinting solution utilizes off-the-shelf Wi-Fi infrastructure and requires no extra hardware in the APs or target devices, there are limitations to consider. The site survey process is time-consuming and labor-intensive. Moreover, to construct the radio map, true location labels are required, which are typically arduous to obtain and correlate with specific fingerprints. For instance, as presented in the experiment in [25], consider a six-story shopping

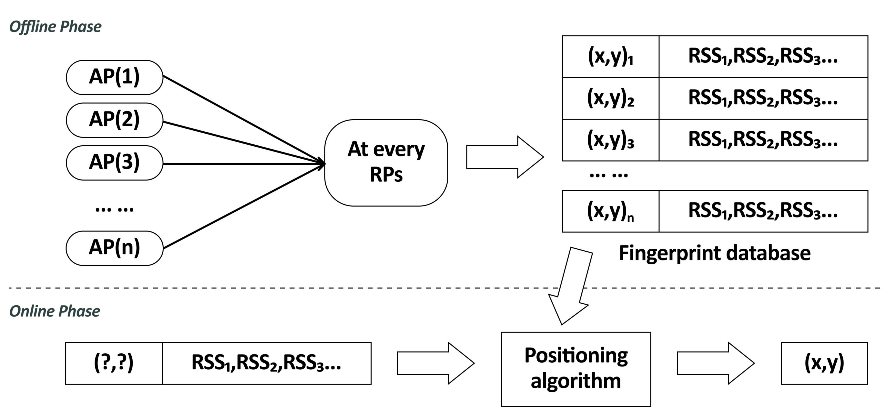

Figure 4: Overview of the Wi-Fi Fingerprint Method [24]. During the offline phase, Received Signal Strength (RSS) are collected at every Reference Points (RPs) from all Access Points (APs). The $(x, y)_i$ are the coordinates of RPs. During the online phase, the user's location is estimated based on an algorithm to find the closet match between the real-time RSS and the data entries in the database.

mall spanning approximately 36,000 m^2, it would require a team of three individuals ten days to collect the Wi-Fi signal readings at a granularity of $5m \times 5m$. This labor-intensive process proves to be unscalable for large-scale deployment.

Several recent studies have suggested crowd-sourcing as a way to minimize the need for site survey, allowing users to generate, adjust and utilize location data created by others [22]. [26] enhanced the crowd-sourcing approach by introducing a new algorithm to tackle challenges arising from user inputs, such as maintaining data quality in a dynamic fingerprint database, communicating location accuracy to users, optimizing user prompting frequency, and filtering user-provided data for reliability. Nonetheless, requesting immediate feedback from users can be inconvenient and disruptive to the user experience. To alleviate user burden, recent research [21] suggested mapping collected RSS fingerprints onto the indoor map during users' daily walk. This approach eliminates the need for intensive data collection by users and obviates the necessity for specialized site surveys. Nevertheless, this method still faces challenges as the quality of fingerprint collection may be compromised by noisy measurements and biased user inputs [27]. Other studies such as the one by [28] leveraged a 3D ray-tracing technique to simulate RSS propagation throughout the area. [29] developed an RSS-based augmentation technique that randomly selects RSS values at reference points, augmenting the dataset size while maintaining original data patterns to improve the performance of deep learning classifiers in site survey scenarios.

To date, fingerprinting-based methods remain the only Wi-Fi indoor localization technique deployed in real-world applications [25], as they do not impose any requirements on Wi-Fi access points and do not rely on side information such as time.

2.4 Time Reversal Resonating Effect

As introduced in Subsection 2.2, Channel Charting leverages channel features to reconstruct the users' locations in a channel chart. The quality of the channel chart relies heavily on dissimilarities used between channel features [30]. Recent research by [31] compares the localization results between Channel Charting and Fingerprinting methods, revealing that despite Channel Charting's advantage of not requiring ground truth labels, its localization accuracy currently lags behind Fingerprinting. This limitation in chart reconstruction capability motivates the present research, which proposes a new dissimilarity metric based on the Time Reversal Resonating Effect to generate more accurate charts for localization and other applications.

Time Reversal Resonating Effect (TRRE) represents a fundamental physical phenomenon that enables precise focusing of electromagnetic waves in complex propagation environments [32]. First demonstrated experimentally with electromagnetic waves in the GHz range [33], TRRE showcases how a time-reversed wave can converge back to its original source with both spatial and temporal compression as shown in Figure 5a, making it particularly valuable for wireless communications and localization applications.

TRRE provides a powerful framework for Channel Charting applications through its inherent ability to characterize spatial relationships between transmitters and receivers. The phenomenon exhibits distinct properties that make it particularly suitable for spatial mapping. First, the multipath profile at each location creates a unique signature due to the specific combination of reflections and scattering paths, ensuring location specificity. Second, time-reversed signals from spatially proximate positions exhibit strong correlation, while distant positions show weak correlation, enabling reliable spatial discrimination. Third, the technique naturally adapts to the complexity of the propagation environment, with performance often improving in rich multipath scenarios. These characteristics enable the construction of reliable distance metrics for manifold learning without requiring explicit position information, forming the basis for unsupervised spatial mapping in Channel Charting applications.

2.4.1 Physical Principles

The time reversal process consists of two distinct phases: the channel probing phase and the time reversal transmission phase. In the channel probing phase, a source transmits a short electromagnetic pulse that propagates through a complex medium. During propagation, the signal undergoes multiple reflections, refractions, and scattering events, creating a rich multipath environment. A receiving antenna captures this reverberated signal, which typically exhibits a significantly longer duration than the original pulse due to multiple path delays [34].

In the time reversal transmission phase, the captured signal is time-reversed and retransmitted through the same environment. Due to channel reciprocity and temporal stationarity, the time-reversed wave retraces its incoming paths and converges back to the initial source location. This convergence manifests in two primary effects: spatial focusing and temporal focusing. The spatial focusing effect results in signal power forming a sharp peak at the intended location while remaining

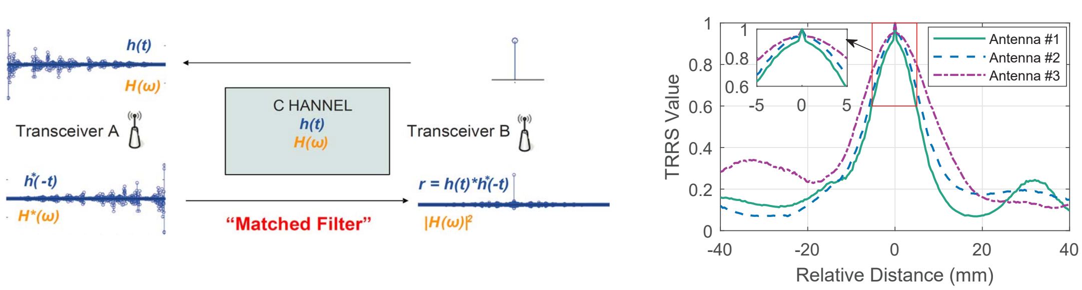

(a) TR signal processing principle [34]

(b) Self-TRRS [32]

Figure 5: TRRE Principle Illustration

relatively low elsewhere, as depicted in Fig 5b. This focusing is achieved through constructive interference at the source and destructive interference at other locations. Simultaneously, temporal focusing occurs as the received signal is compressed in time, recovering approximately the duration of the original pulse through the coherent combination of multipath components.

2.4.2 Mathematical Representation

For a transmitted signal $m(t)\cos(2\pi f_0 t + \phi(t))$, where f_0 is the carrier frequency, the received signal after propagation through a complex environment can be expressed as:

$$s(t) = m'_I(t)\cos(2\pi f_0 t) + m'_Q(t)\sin(2\pi f_0 t),$$

where $m'_I(t)$ and $m'_Q(t)$ represent the in-phase and quadrature components of the received signal. The time-reversed signal is then constructed as:

$$s(-t) = m'_I(-t)\cos(2\pi f_0 t) - m'_Q(-t)\sin(2\pi f_0 t)$$

This formulation accounts for both the baseband signal components and the carrier wave phase conjugation necessary for effective time reversal.

2.5 Manifold Learning

2.5.1 Manifold Learning Fundamentals

Manifold learning represents a class of dimensionality reduction techniques based on the assumption that high-dimensional data lies on or near a lower-dimensional manifold $\mathcal{M}$ [35]. In the context of Channel Charting, the high-dimensional CSI measurements $\mathbf{H} \in \mathbb{C}^{N_f \times N_t}$ are assumed to form a manifold structure that reflects the physical geometry of the wireless propagation environment. This assumption is particularly relevant because while CSI data exists in a high-dimensional space, the physical locations of transmitters and receivers are confined to a much lower-dimensional space, typically 2D or 3D. The objective of manifold learning is to discover a mapping $f : \mathbb{C}^{N_f \times N_t} \to \mathbb{R}^d$ that preserves the intrinsic geometry of the data while reducing its dimensionality.

2.5.2 Classical Manifold Learning Approaches

Several classical manifold learning techniques have been applied in Channel Charting applications, each with its own strengths and theoretical foundations. Principal Component Analysis (PCA) [36], the most fundamental approach, performs linear projection through eigendecomposition of the covariance matrix:

$$\mathbf{\Sigma} = \frac{1}{N}\sum_{i=1}^{N}(\mathbf{x}_i - \mu)(\mathbf{x}_i - \mu)^\top = \mathbf{U}\mathbf{\Lambda}\mathbf{U}^\top,$$

where $\mathbf{U}$ contains the eigenvectors and $\mathbf{\Lambda}$ the corresponding eigenvalues. While PCA is computationally efficient and theoretically well-understood, its linear nature often fails to capture the nonlinear structure inherent in CSI data.

Multidimensional Scaling (MDS) [37] takes a different approach by focusing on preserving pairwise distances. It minimizes the stress function:

$$\mathcal{L}_{MDS} = \sum_{i,j}(d_{ij} - \|\mathbf{z}_i - \mathbf{z}_j\|_2)^2,$$

where d_{ij} represents the high-dimensional distances and $\mathbf{z}_i$ the low-dimensional embeddings. This approach is particularly valuable in Channel Charting as it directly attempts to preserve spatial relationships between measurements.

Locally Linear Embedding (LLE) [38] introduces a powerful concept of preserving local geometry through a two-step process. First, it computes optimal weights for reconstructing each point from its neighbors:

$$\min_{\mathbf{W}} \sum_i \|\mathbf{x}_i - \sum_j w_{ij}\mathbf{x}_j\|^2 \quad \text{subject to} \quad \sum_j w_{ij} = 1$$

Then, it finds low-dimensional embeddings that preserve these neighborhood relationships:

$$\min_{\mathbf{Z}} \sum_i \|\mathbf{z}_i - \sum_j w_{ij}\mathbf{z}_j\|^2$$

This local approach is particularly effective when the manifold structure is locally Euclidean but globally nonlinear.

2.5.3 Deep Learning-Based Manifold Learning

Modern approaches leverage deep neural networks for nonlinear manifold learning, offering greater flexibility and capacity to learn complex mappings. The autoencoder architecture, a fundamental building block of these approaches, consists of an encoder f_θ and decoder g_ϕ:

$$\mathbf{z} = f_\theta(\mathbf{x}), \quad \hat{\mathbf{x}} = g_\phi(\mathbf{z})$$

These networks are trained to minimize the reconstruction loss while maintaining the essential structure of the data:

$$\mathcal{L}_{AE} = \|\mathbf{x} - g_\phi(f_\theta(\mathbf{x}))\|^2 + \lambda\Omega(\theta, \phi),$$

where $\Omega(\theta, \phi)$ represents regularization terms that can enforce desired properties such as smoothness or sparsity in the learned representations.

Siamese networks [39] extend this framework by explicitly incorporating pairwise similarity relationships during training. They employ a contrastive loss:

$$\mathcal{L}_{contrast} = yd(\mathbf{z}_1, \mathbf{z}_2) + (1 - y)\max(0, m - d(\mathbf{z}_1, \mathbf{z}_2))$$

where y indicates whether pairs are similar, d is a distance metric, and m is a margin parameter. This architecture is particularly well-suited for Channel Charting as it can learn to preserve relative spatial relationships between CSI measurements.

2.5.4 Distance Preservation in Manifold Learning

The preservation of distance relationships is formalized through the concept of isometry, which provides a theoretical framework for evaluating the quality of the learned manifold. A mapping f is considered isometric if:

$$d_{\mathcal{M}}(\mathbf{x}_1, \mathbf{x}_2) \approx \alpha d_{\mathbb{R}^d}(f(\mathbf{x}_1), f(\mathbf{x}_2)),$$

where $d_{\mathcal{M}}$ is the geodesic distance on the manifold, $d_{\mathbb{R}^d}$ is the Euclidean distance in the embedded space, and α is a scaling factor. This property ensures that spatial relationships in the original space are maintained in the lower-dimensional representation.

In practice, the geodesic distance can be approximated using shortest paths in a neighborhood graph:

$$d_G(\mathbf{x}_i, \mathbf{x}_j) = \min_{\text{path}(i \to j)} \sum_{(k,l) \in \text{path}} \|\mathbf{x}_k - \mathbf{x}_l\|_2$$

This approximation is particularly useful in Channel Charting as it can capture the intrinsic structure of the wireless propagation environment.

3 Related Work

3.1 Evolution of Channel Charting

Channel Charting represents a significant advancement in wireless communications, offering a self-supervised learning framework for spatial awareness without explicit position information. The foundational work by [13] introduced the core concept of learning spatial relationships directly from CSI measurements, demonstrating the feasibility of dimensional reduction from complex CSI space to physical coordinates. This initial research established a two-stage pipeline: first computing a dissimilarity matrix through pairwise comparisons of CSI samples, then obtaining low-dimensional embeddings through manifold learning techniques.

The applications of Channel Charting have expanded across multiple domains, including indoor user localization [1], radio resource management [2], and millimeter wave beam management [3]. Recent work by [4] has further demonstrated its potential in 5G and beyond networks, particularly for ultra-reliable low-latency communications and enhanced mobile broadband services.

3.2 CSI-based Dissimilarity Metrics

The development of CSI-based dissimilarity metrics has progressed through several generations of approaches. The initial Channel Charting implementation proposed a metric derived from the Euclidean distance between feature matrices extracted from CSI [13], assuming path loss proportionality to physical proximity. While this approach enabled basic reconstruction of radio environments using techniques like Sammon's mapping and PCA, it showed limitations in non-collinear measurement scenarios.

Subsequent research addressed these limitations through more sophisticated metrics. The work by [14] introduced a cosine-based dissimilarity measure designed to be resilient against small-scale fading effects. Further advancements came from [30], which proposed a correlation matrix distance (CMD)-based metric capable of filtering geometrically inconsistent measurement combinations before dimensionality reduction.

Alternative approaches have explored clustering-based metrics. Research by [40] introduced metrics based on multipath component clustering, leveraging the observation that proximate user equipment shares similar multipath characteristics. This concept was further developed by [41], who proposed operating directly on channel impulse responses (CIRs) for improved accuracy.

3.3 Side Information-based Dissimilarity Metrics

The integration of external side information has emerged as a significant direction in improving distance estimation accuracy. Research by [42] established the correlation between spatial and temporal proximity, leading to the development of time-based metrics [43, 44, 45]. These approaches typically assume linear trajectories with constant velocity, though this assumption can limit their practical applicability.

Recent work has attempted to overcome these limitations through more sophisticated side information. The research by [31] introduced a velocity-aware metric utilizing data from Pedestrian Dead Reckoning (PDR) systems or robotic odometry. While this approach reduces dependence on motion assumptions, it introduces additional hardware requirements at the user end.

3.4 CSI-based Moving Distance as a Dissimilarity Metric

A key innovation in Channel Charting involves the use of moving distance as a fundamental dissimilarity metric. This approach differs from traditional methods that rely on direct CSI comparison or signal strength patterns. By accurately estimating the physical distance traveled between measurement points, the resulting channel charts better preserve spatial relationships in the environment.

The Time Reversal Resonating Effect (TRRE) provides one effective mechanism for estimating moving distances from CSI measurements. Through careful analysis of the Time Reversal Resonating Strength (TRRS) patterns, accurate distance estimates can be derived without requiring additional sensors or motion constraints [46, 32]. As shown in Figure 5b, spatial divergence of less than 10 mm can result in TRRS value reductions exceeding 0.7, indicating exceptional spatial sensitivity.This represents a significant advance over previous approaches that either required supplementary hardware or imposed restrictive assumptions about user movement.

TRRE applications span various localization tasks. Research by [46] applied TRRS to individual gait recognition, while [47] demonstrated its effectiveness in passive human speed estimation. Significant work by [32] and [48] has shown TRRE's utility in indoor tracking applications, achieving high accuracy without specialized hardware requirements.

While existing Channel Charting approaches have shown promise, they face persistent challenges. CSI-based metrics often struggle with environmental sensitivity, while side-information approaches typically require additional hardware or impose restrictive motion assumptions. TRRS has emerged as a potential solution, offering millimeter-level precision and robust spatial correlation properties without hardware dependencies.

The present research represents the first systematic effort to adapt TRRS as a fundamental dissimilarity metric for Channel Charting. This approach bridges the gap between theoretical time-reversal principles and practical radio environment mapping, offering potential advantages over conventional path-loss and CSI-based methods in complex multipath environments. The integration of TRRS principles with Channel Charting frameworks presents an opportunity to overcome existing limitations while maintaining system simplicity and hardware independence.

4 Methodology

This section presents a novel approach to Channel Charting that leverages TRRS-derived Moving Distance as a fundamental metric for constructing reliable spatial relationships between wireless channel measurements. The proposed methodology comprises four primary components: pair-wise Moving Distance calculation based on TRRS, dissimilarity matrix construction, further matrix enhancement, and lastly manifold learning for dimensional reduction. Each component addresses specific challenges in creating an accurate and robust channel chart while maintaining computational efficiency.

4.1 Pair-wise Moving Distance Calculation

4.1.1 Time Reversal Resonating Strength (TRRS) Calculation

The foundation of the proposed methodology lies in exploiting the Time Reversal Focusing Effect, a physical phenomenon that enables precise spatial discrimination in complex propagation environments. Time Reversal (TR) represents a fundamental physical resonance mechanism that concentrates transmitted signal energy at an intended focal point in both temporal and spatial domains through the transmission of the TR waveform [48]. Within the context of Wi-Fi channels, the received CSI exhibits constructive interference when merged with its time-reversed and conjugate equivalent at the intended position, while producing incoherent responses at other locations [32].

The quantification of this focusing effect is achieved through TRRS, which serves as a metric for assessing the spatial correlation between pairs of CSI measurements. In a typical measurement scenario, a transmitter continuously emits signals omnidirectionally while a receiver traverses from position $\vec{R}_0$ to $\vec{R}_t$. The TRRS between CSI measurements at these two locations is computed using:

$$\kappa(H_1, H_2) = \frac{|H_1^H H_2|^2}{< H_1, H_1 >< H_2, H_2 >}$$

where H_1 and H_2 represent the Channel Frequency Responses (CFR) at the respective positions. For a dataset collected by a mobile platform, TRRS values are computed between consecutive CFR measurements and stored for subsequent analysis.

The raw TRRS measurements exhibit a characteristic Bessel-function-like pattern, as illustrated in Figure 6. However, measurement noise introduces outliers that can complicate peak detection. To enhance measurement reliability, the raw TRRS data undergoes preprocessing through low-pass filtering and outlier removal. The comparative results before and after processing, presented in Figure 6, demonstrate significant improvement in signal quality and peak detectability.

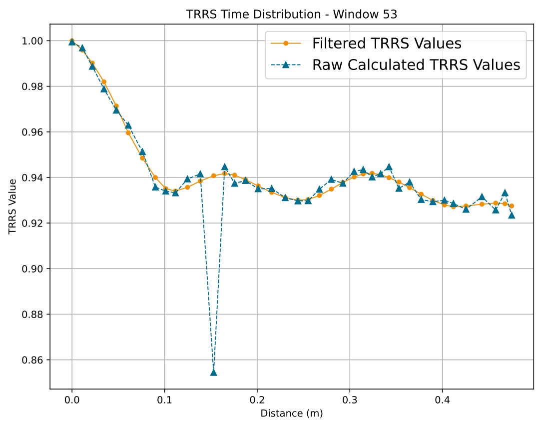

(a)

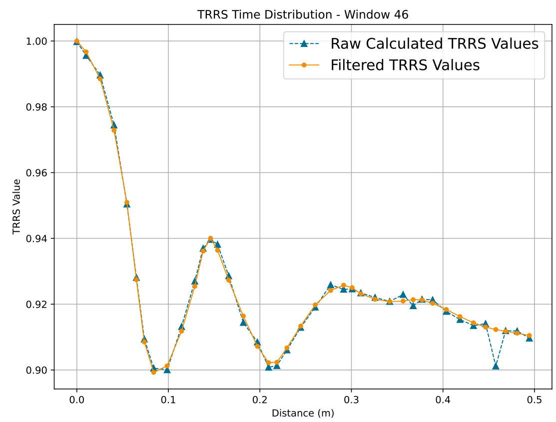

(b)

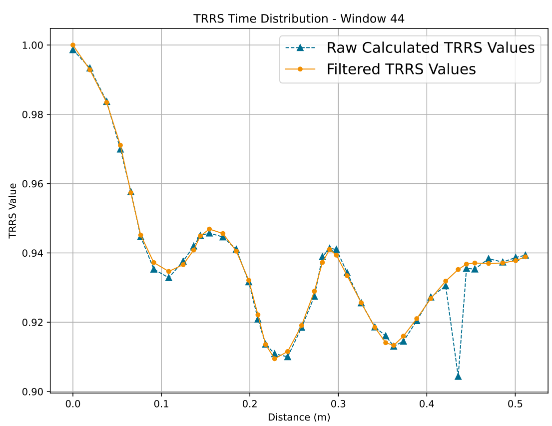

(c)

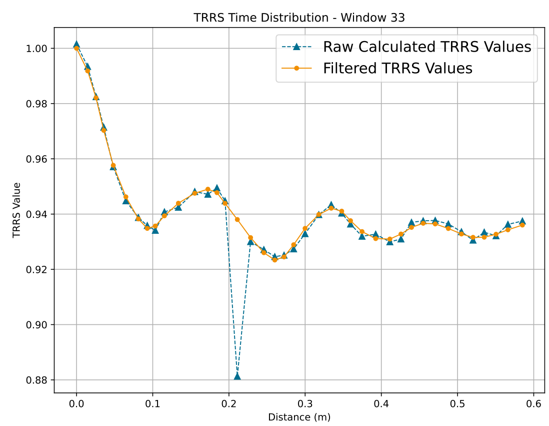

(d)

Figure 6: Spatial Relative TRRS values computed for selected data windows. The plot compares raw data (blue) with filtered data (orange) to highlight the effect of the filtering process on signal stability and trend clarity.

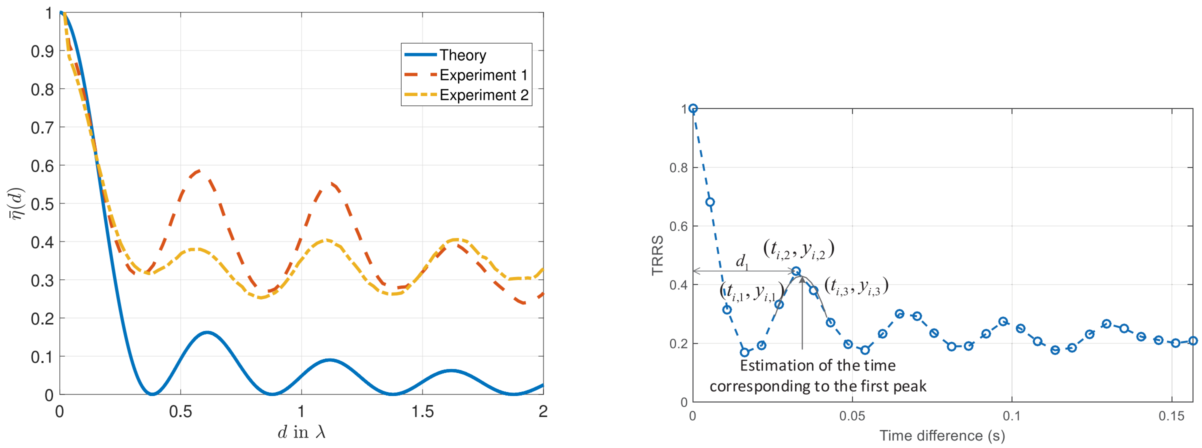

(a) Spatial Distribution

(b) Time Distribution

Figure 7: Spatiotemporal distribution of TRRS values [48].(a) Comparison between experimental TRRS distributions (Experiments 1 and 2) and the theoretical model; (b) Visualization of the TRRS-based speed estimation algorithm.

4.1.2 Speed Estimation from TRRS Patterns

The Time Reversal focusing effect manifests distinctly in both spatial and temporal domains, as evidenced in Figure 7. Analysis of these distributions reveals consistent damping patterns that form the basis for speed estimation. A key observation lies in the initial local peak of $\eta(d)$, which occurs at a theoretical distance d_0 of approximately 0.6λ, following the Bessel-function-like structure. Speed estimation requires determining the time $\hat{t}$ taken for the receiver to traverse from its initial position to this primary peak. By approximating the peak region with a quadratic curve and utilizing the timestamps associated with each Channel Impulse Response (CIR) measurement, $\hat{t}$ can be determined through vertex identification. The speed estimation then reduces to:

$$\hat{v} = \frac{d_0 \lambda}{2\pi \hat{t}}, \tag{1}$$

where λ is the wavelength.

The processing pipeline implements a two-stage approach for identifying characteristic TRRS peaks. Initial processing employs Gaussian smoothing followed by established peak detection algorithms. While this approach proves effective for well-defined patterns (Figures 8a & 8b), it encounters limitations when processing windows exhibit low signal-to-noise ratios (Figure 8c), where damping patterns lack sufficient prominence for reliable detection.

To address these limitations, a secondary zero-crossing detection method has been implemented to capture subtle peaks that elude conventional detection methods. The selection of window size represents a critical trade-off between peak detection reliability and temporal resolution. Empirical analysis has established an optimal window size of 40 samples, which effectively balances these

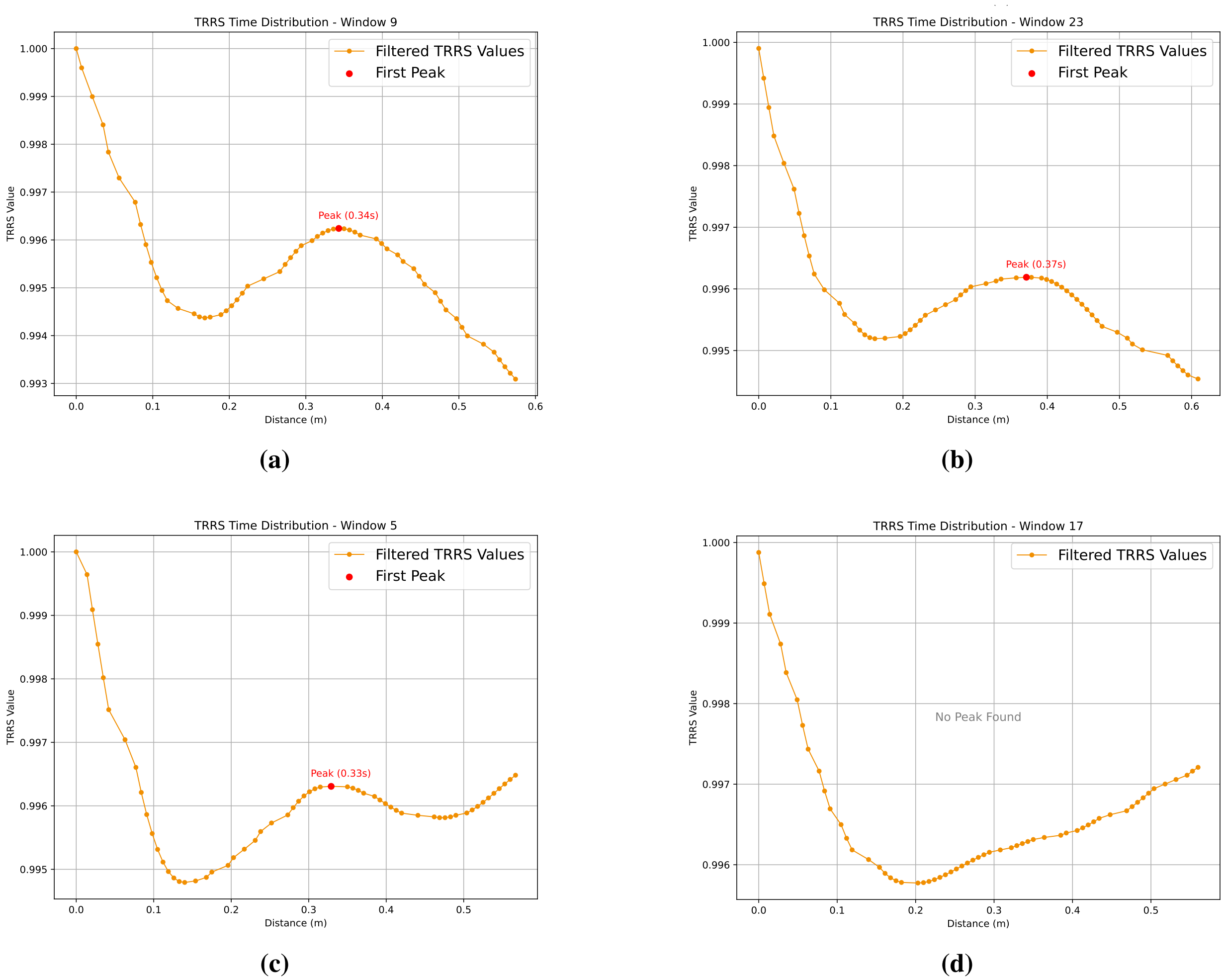

Figure 8: Performance of the peak detection algorithm across different channel conditions. (a–b) Clear and distinct peaks accurately detected using standard methods; (c) Low-SNR scenario where zero-crossing analysis was necessary for robust peak identification; (d) Challenging case with no discernible peak structure, resulting in an unusable measurement window.

competing requirements.

A notable challenge arises from windows that fail to yield detectable peaks, approximately 5.0325% of the total dataset (Figure 8d). After extensive evaluation of potential mitigation strategies, including endpoint approximation and model-based imputation, the methodology adopts a conservative approach of excluding these problematic windows. This design choice prioritizes measurement accuracy over dataset completeness, ensuring that only high-confidence measurements contribute to the final speed estimates.

4.2 Dissimilarity Matrix Construction

Given the estimated walking speed v, the calculation of moving distances requires determining the time interval between consecutive CSI measurements. The dataset provides precise timing information for each measurement, enabling the computation of moving distances through:

$$\hat{d}_x = \sum_{i=0}^{n_x} \hat{v}_i \cdot \Delta t, \tag{2}$$

where $\hat{v}_i$ is the velocity calculated using Eqn. (1), Δt is the selected time window, and n_x represents the number of key points inside the time window for distance calculation.

These pair-wise distances form an $N \times N$ dissimilarity matrix, where N represents the total number of data samples. The dataset structure presents a particular challenge, as it contains several independent traces separated by significant time gaps. In these cases, TRRS values do not reflect meaningful spatial correlations between traces. Consequently, the pair-wise moving distances must be calculated independently for each trace, resulting in a sparse dissimilarity matrix where inter-trace distances are set to zero to indicate unreliable measurements.

The relationship between calculated moving distances and actual Euclidean distances requires careful consideration. When the ground truth path follows a ”zig-zag” pattern, the calculated moving distance may significantly exceed the Euclidean distance, potentially leading to distortions in the reconstructed channel chart (Figure 9). To mitigate this effect, an empirically determined distance threshold of 60 meters has been established. Only TRRS-derived moving distances between points from the same trace with ground truth distances below this threshold are considered valid for the dissimilarity matrix.

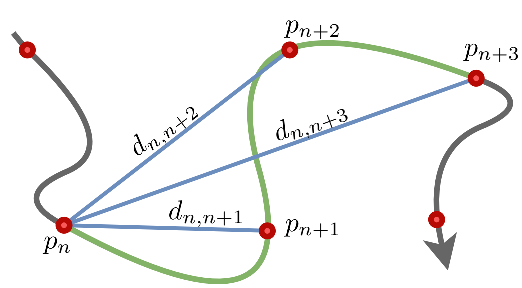

Figure 9: Agent trajectory illustrated through consecutive CSI measurements, represented by red dots [45]. This visualization highlights the relationship between the agent's physical movement and the corresponding changes in Euclidean distance within the CSI feature space.

4.3 Metric Fusion and Enhancement

The sparse nature of the TRRS-derived dissimilarity matrix presents challenges for manifold learning, as the limited number of valid distance measurements reduces the available geometric constraints. To address this limitation, the methodology incorporates cosine dissimilarity as a complementary metric. First proposed by [14], the cosine-based metric provides direct similarity measurements between CSI data points. For MIMO systems, this dissimilarity can be computed across antenna arrays and subcarriers:

$$d_{CS,i,j} = \sum_{b=1}^{B}\sum_{n=1}^{N}\left(1 - \frac{|\sum_{m=1}^{M}(\mathbf{H}_{b,m,n}^{(i)})^{*}\mathbf{H}_{b,m,n}^{(j)}|^{2}}{\left(\sum_{m=1}^{M}|\mathbf{H}_{b,m,n}^{(i)}|^{2}\right)\left(\sum_{m=1}^{M}|\mathbf{H}_{b,m,n}^{(j)}|^{2}\right)}\right)$$

To ensure balanced contribution from both metrics, the cosine dissimilarity undergoes normalization to match the scale of the moving distance metric. This fusion strategy enhances the robustness of the final channel chart by incorporating complementary spatial information from both TRRS-based and cosine-based measurements.

4.4 Neural Network Architecture and Training

The dimensional reduction component of the methodology employs two complementary neural network architectures: Siamese and Triplet networks (Figure 10). As shown in Figure 10a, the structure of a Siamese neural network consists of twin networks with shared weights, processing pairs of CSI measurements simultaneously to learn a mapping that preserves relative spatial relationships. Triplet neural network (Figure 10b) provides another powerful network structure for Channel Charting. Both architectures share a common feature extraction backbone while differing in their training objectives and sample organization strategies.

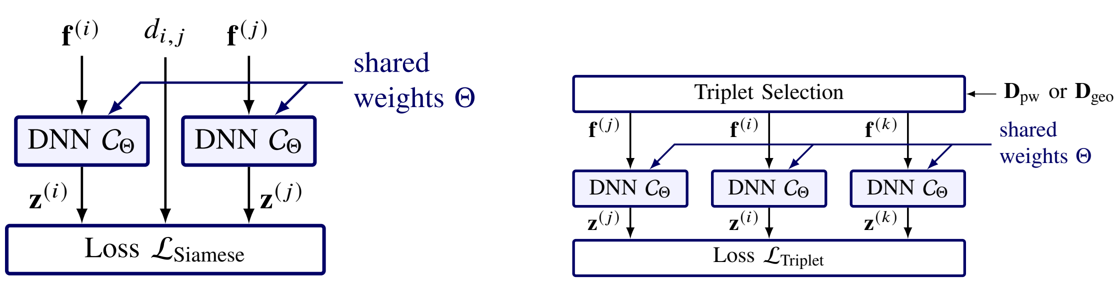

(a) Siamese neural network structure

(b) Triplet neural network structure

Figure 10: Comparison of deep metric learning architectures [10]. (a) Structure of a Siamese neural network, which learns to measure similarity between input pairs; (b) Structure of a Triplet neural network, which learns to differentiate between anchor, positive, and negative samples for embedding space separation.

4.4.1 Feature Engineering and Network Architecture

The network's feature extraction pipeline consists of three main components. The first component implements a specialized autocorrelation computation for the Feature Engineering Layer:

$$S_{mn}(t) = \sum_{d} \mathrm{CSI}_{d,m,t} \cdot \mathrm{CSI}^{*}_{d,n,t}$$

where (m, n) index the antenna arrays and t represents the time index. The output preserves both real and imaginary components of the autocorrelation.

The second component comprises a Dense Network Stack with a sequence of fully-connected layers and batch normalization. The network processes a flattened feature vector of dimension $(N_a \times N_a \times N_t \times 2)$ through successive layers of decreasing size: 1024, 512, 256, 128, and 64 nodes, with ReLU activation functions throughout. The final layer produces a 2-dimensional embedding suitable for visualization and subsequent analysis.

The third component implements architecture-specific distance computations necessary for loss calculation, enabling effective training of both Siamese and Triplet configurations.

4.4.2 Training Strategy and Optimization

The methodology implements two complementary training approaches. The Siamese Network training processes pairs of CSI measurements (A, B) using a combined loss function that incorporates both TRRS and cosine dissimilarity:

$$\mathcal{L}_{Siamese} = w_1 \mathcal{L}_{TRRS} + w_2 \mathcal{L}_{cosine}$$

with weights $(w_1, w_2) = (0.4, 0.6)$ determined through empirical validation.

The Triplet Network training processes triplets (anchor, positive, negative) using a margin-based triplet loss:

$$\mathcal{L}_{Triplet} = \max(0, \|f(a) - f(p)\|^2 - \|f(a) - f(n)\|^2 + \text{margin})$$

with a margin parameter of 0.005.

4.4.3 Sample Selection and Training Process

The training process employs sophisticated sample selection strategies to ensure effective learning. For Siamese pair selection, the process maintains balance between same-trace and cross-trace pairs while incorporating both TRRS-based moving distance and cosine-based dissimilarity measures. The batch size is set to 4 pairs per batch to optimize computational efficiency and learning stability.

For Triplet selection, positive samples are selected based on a dissimilarity threshold set at the 40th percentile, while negative samples are chosen above the 60th percentile dissimilarity. This range-aware selection strategy maintains trace coherence and ensures meaningful learning signals.

The optimization framework utilizes the AdamW optimizer with an initial learning rate of 0.001. A step-based learning rate schedule is implemented with a step size of 10 epochs and a decay factor of 0.8, continuing for a total of 25 epochs. The training process includes careful monitoring of loss metrics:

$$\text{Epoch Loss} = \frac{1}{N_b} \sum_{i=1}^{N_b} \mathcal{L}_i$$

This comprehensive approach, combining sophisticated architecture design, careful sample selection, and robust optimization strategies, enables effective learning of spatial relationships while maintaining computational efficiency. The complementary nature of Siamese and Triplet networks provides redundancy in learning spatial relationships, while the careful sample selection ensures effective use of available training data.

5 Results

This section presents two primary results: the moving distance estimation accuracy and the generated channel charts.

The analysis utilizes the DICHASUS dataset [49], which comprises CSI data encompassing both line-of-sight and non-line-of-sight indoor scenarios. The experimental setup consists of 32 antennas positioned at the four corners of an L-shaped region, functioning as receivers. A mobile robot equipped with a single antenna serves as the transmitter, moving randomly within this predefined area.

5.1 Moving Distance Estimation

The first phase of Channel Charting evaluates the accuracy of calculated moving distances between CSI data points. The dataset contains three independent traces with distinct trajectory shapes, as illustrated in Figure 11. The traces exhibit total lengths of $233.7686, 285.7500,$ and $494.6165m$ respectively. Later results reveals that Trace 3 demonstrates significantly larger errors compared to the other two traces, potentially due to its higher frequency of sharp turns. The "zig-zag" shape characteristic of Trace 3 represents a challenging scenario for the proposed methodology.

The evaluation metrics demonstrate promising results across all traces. The Mean Squared Error (MSE) achieves $0.1691m$ while the Mean Absolute Error (MAE) reaches $0.2932m$. Figure 12 presents the CDF of MAE for each trace, with 50th percentile errors of $0.74, 0.76,$ and $0.97m$ respectively. These results validate the effectiveness of the moving distance calculation algorithm even under challenging movement patterns.

Beyond trajectory shape considerations, accumulated error represents another critical factor in performance evaluation. Figure 13 illustrates the temporal evolution of estimation error along each trajectory. While Trace 3 exhibits higher error rates (averaging $0.4m$ for the initial 250 seconds),

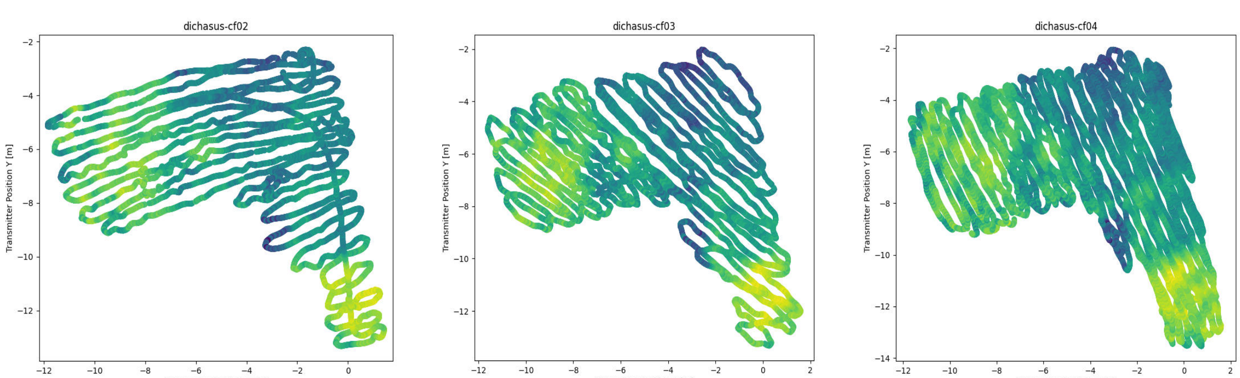

Figure 11: Three distinct trajectories from the dataset used for analysis

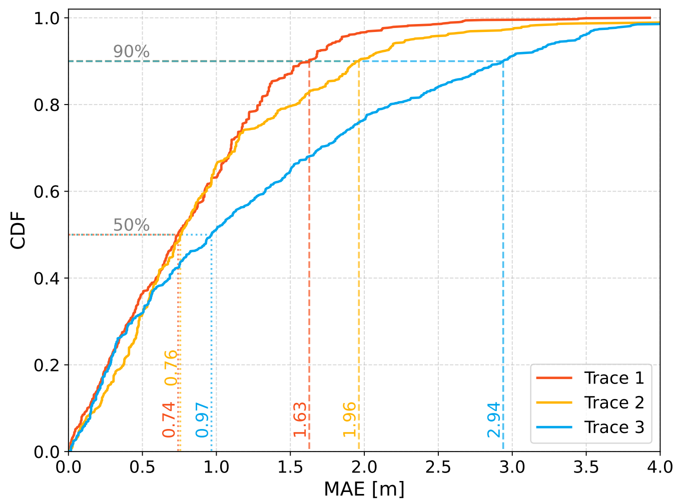

Figure 12: Cumulative distribution function (CDF) of mean absolute error (MAE) for three trajectory traces.The plot highlights the 50th (median) and 90th percentile error values to compare localization performance across traces.

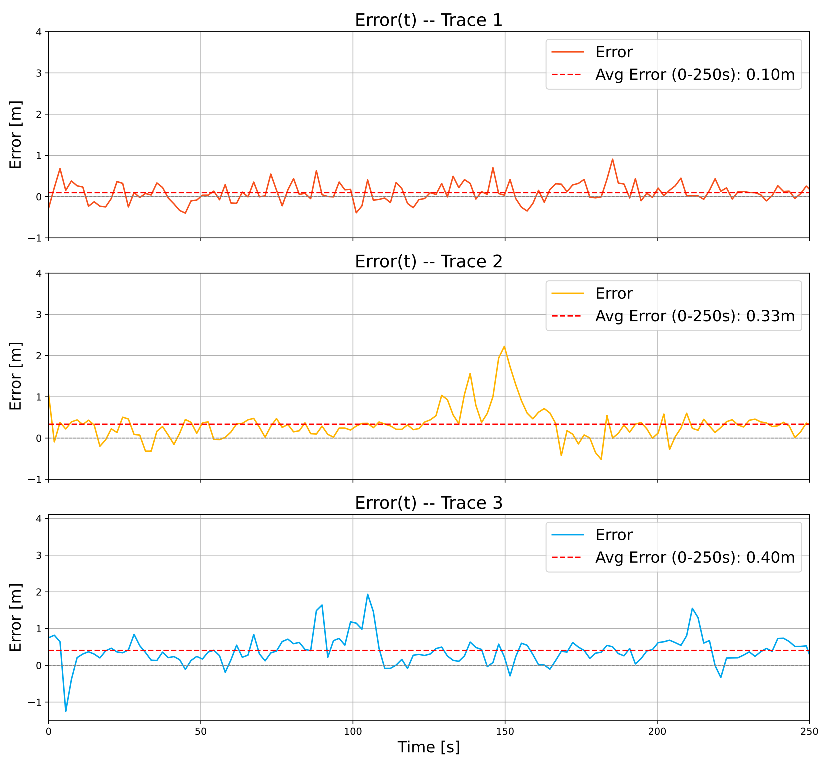

Figure 13: Estimation error over time across a 250-second interval, illustrating the temporal dynamics and stability of the performance of the proposed algorithm.

the overall error magnitude remains within acceptable bounds.

The training process employs random data pair selection rather than sequential distance calculations. Figure 14 presents an analysis of 1000 randomly selected data pairs from each trace, comparing estimated moving distances with ground truth measurements. To mitigate accumulated error and minimize trajectory-dependent effects, the analysis considers only data pairs with ground truth distances below $60m$.

Figure 14a provides an aggregate view of the results across all traces, while subsequent plots detail the performance for each individual trace. In these visualizations, scatter points represent data pairs with ground truth spatial distances on the x-axis and estimated distances on the y-axis. The ideal case of perfect estimation is represented by the diagonal line ($y = x$), shown as a dashed line. The solid line indicates the mean estimated distance for each ground truth distance value, with shaded regions representing one standard deviation of variation. The results demonstrate particularly strong performance at shorter distances, where estimated moving distances closely align with ground truth values and exhibit minimal deviation. This observation underscores the importance of appropriate data pair selection in the methodology.

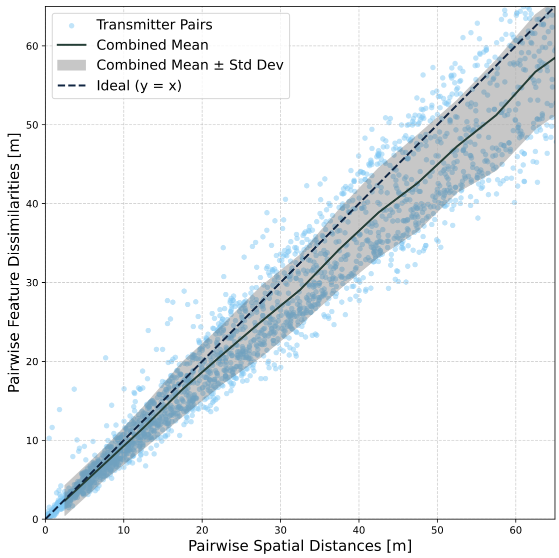

(a) Aggregate view of feature dissimilarity versus ground truth distance across all transmitter pairs. The diagonal line ($y = x$) represents perfect estimation.

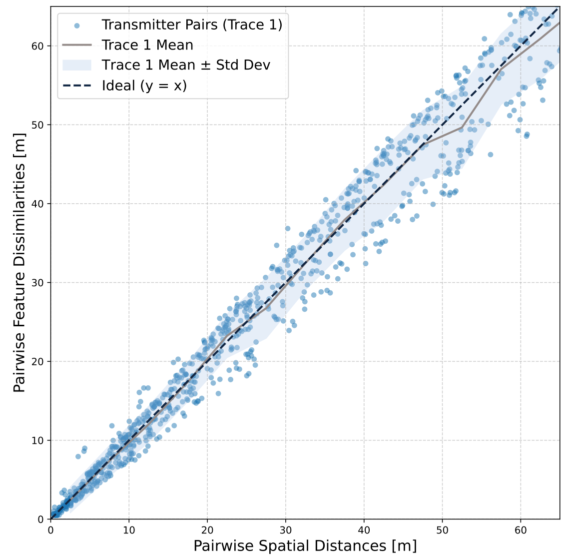

(b) Moving Distance Estimation Error Analysis for Trace 1

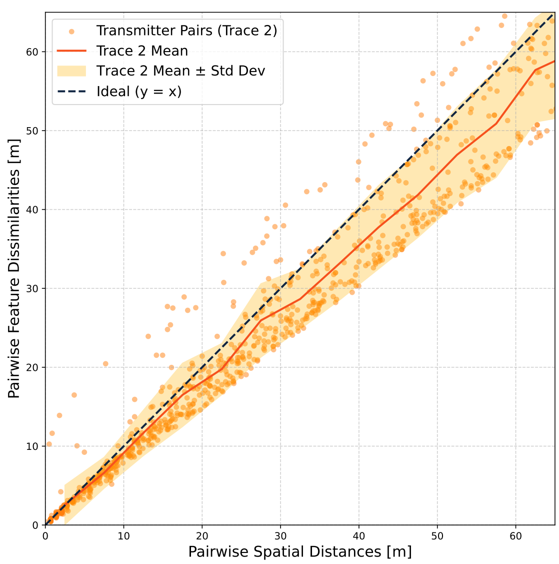

(c) Moving Distance Estimation Error Analysis for Trace 2

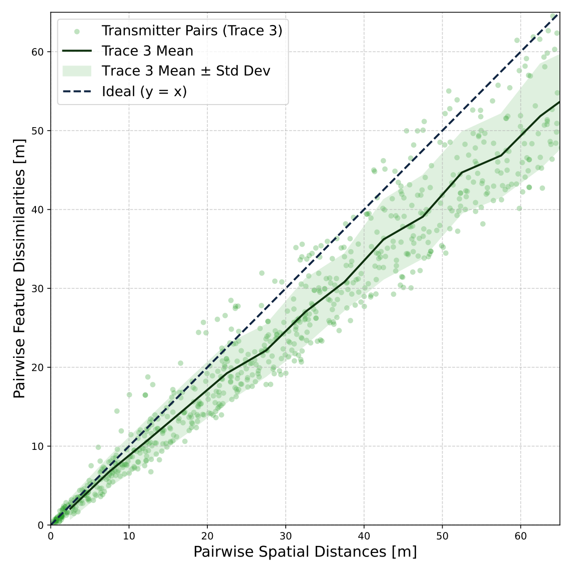

(d) Moving Distance Estimation Error Analysis for Trace 3

Figure 14: Performance analysis of TRRS-based distance estimation. (a) Overview of all measurements across traces; (b–d) Detailed analysis of individual traces, with binned mean values shown as solid lines and shaded areas representing $\pm 1\sigma$ confidence intervals. Color intensity reflects point density, with darker regions indicating higher sample concentration.

5.2 Channel Charts Generation

The second phase of evaluation focuses on the generation and assessment of channel charts using the constructed dissimilarity matrix. The analysis examines both the qualitative preservation of spatial relationships and quantitative performance metrics across different manifold learning approaches.

5.2.1 Qualitative Analysis

Figures 15a and 15c present the channel charts generated using the proposed TRRS-based dissimilarity metric with Siamese and Triplet neural network architectures, respectively. Comparison with the ground truth positions (Figure 15b) reveals several significant characteristics of the generated charts. The charts demonstrate strong preservation of local spatial relationships, evidenced by the gradual color transitions that correspond to physical proximity in the original space. Furthermore, the characteristic L-shaped structure of the measurement environment is successfully captured in both neural network implementations, indicating effective preservation of global geometric features. The density and distribution of points in the generated charts maintain relative consistency with the ground truth, suggesting balanced dimensional reduction without significant clustering artifacts.

For comparative analysis, Figure 15d presents a channel chart generated using the Angle-Delay Profile (ADP) dissimilarity metric. The ADP-based chart exhibits significant geometric distortion, manifesting as a circular structure that bears little resemblance to the ground truth configuration. This limitation of pure ADP-based mapping highlights the advantages of the proposed TRRS-based approach, which achieves superior spatial representation without requiring additional temporal information or geodesic enhancement.

It is noteworthy that the coordinate values in the generated charts differ from the ground truth plot. This discrepancy is an inherent characteristic of manifold learning techniques, as the learned representations may undergo arbitrary rotation, scaling, reflection, or translation while preserving relative spatial relationships [10]. In practical applications, this ambiguity can be resolved through minimal landmark-based calibration.

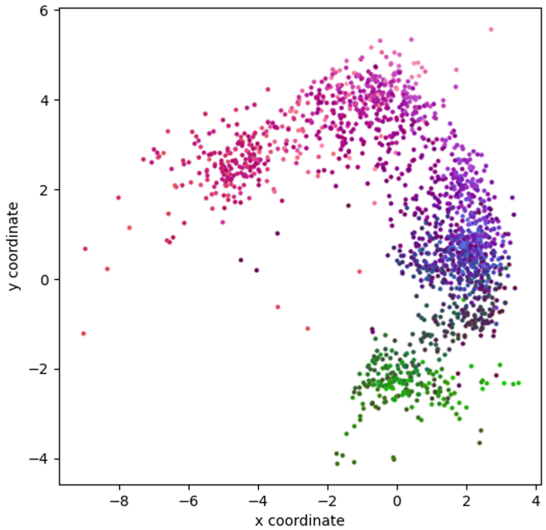

(a) Channel Chart generated by Siamese Model

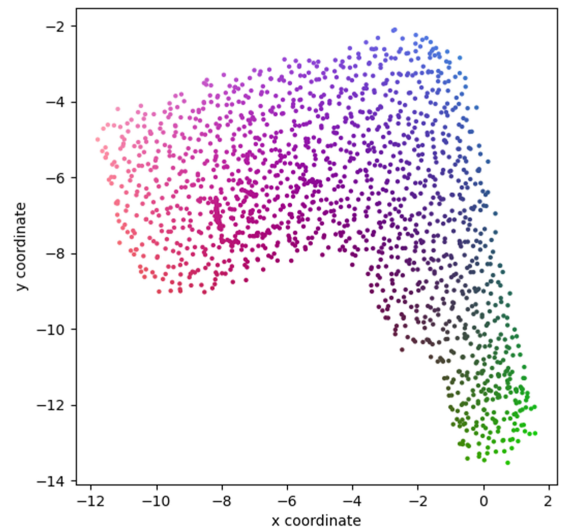

(b) Ground Truth Data Point Positions

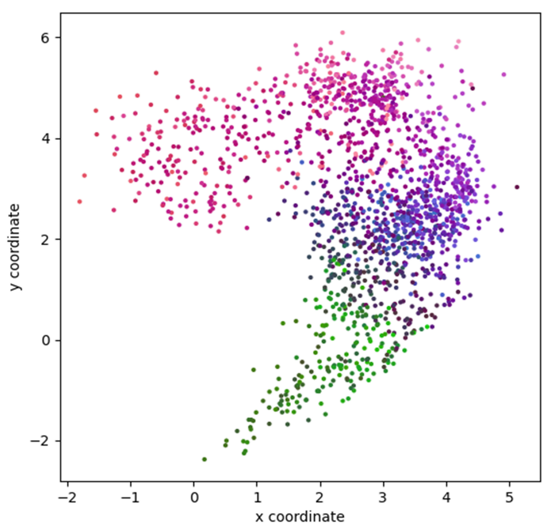

(c) Channel Chart generated by Triplet Model

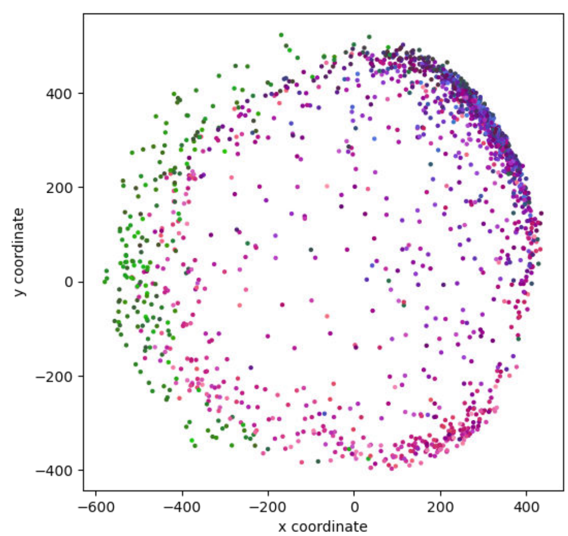

(d) Channel Chart generated using ADP dissimilarity

Figure 15: Comparison of channel charts generated using various deep learning-based manifold learning techniques. (a) and (c) show the channel charts generated by the Siamese and Triplet models, respectively; (b) illustrates the ground truth positions for reference. (d) displays the channel chart generated by the Siamese model using Angle-Delay Profile (ADP) dissimilarity.

5.2.2 Quantitative Performance Evaluation

The quantitative assessment employs three established metrics for evaluating the quality of dimensional reduction. Continuity (CT) measures the preservation of local neighborhood relationships, while Trustworthiness (TW) evaluates the reliability of preserved proximity relationships. Both metrics are bounded in the range $[0, 1]$, with values approaching 1 indicating superior preservation of local relationships. The third metric, Kruskal's Stress (KS), assesses the preservation of global structure and is bounded in $[0, 1]$ with lower values indicating better preservation of global structure.

Figure 16 presents a comparative analysis of these metrics across three approaches: the proposed TRRS-based method, ADP dissimilarity, and Euclidean distance baseline. The analysis reveals superior performance of the TRRS-based approach across all metrics. The method achieves higher CT and TW values, indicating better preservation of local spatial relationships, while simultaneously maintaining lower KS values compared to both ADP and Euclidean baselines, suggesting improved retention of global structure. This consistent performance advantage across all metrics validates the robustness of the TRRS-based dissimilarity measure.

These quantitative results, combined with the qualitative observations, provide strong evidence for the effectiveness of the proposed TRRS-based Channel Charting methodology in preserving both local and global spatial relationships without reliance on additional side information or computational enhancement techniques.

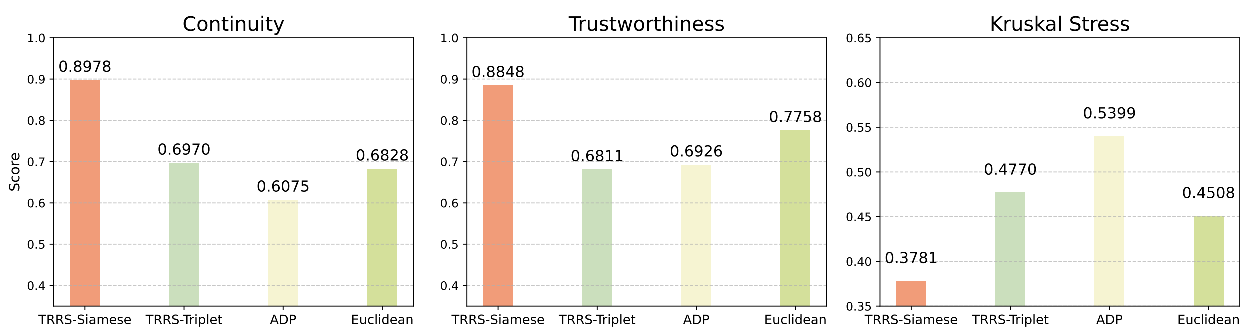

Figure 16: Continuity, Trustworthiness and Kruskal's Stress Evaluation

6 Future Plan and Conclusion

6.1 Future Research Directions

The successful implementation of TRRS-based Channel Charting opens several promising avenues for future research:

6.1.1 Dataset Enhancement and Validation

A primary direction for future work involves the collection and analysis of new datasets with optimized trajectory patterns. The current public datasets, while valuable, contain trajectories that may not fully showcase the potential of the TRRS-based moving distance approach. Future research should focus on expanding the dataset diversity through the collection of data with varied movement patterns, enabling more comprehensive evaluation of the TRRS-based moving distance metric's robustness. Additionally, the integration of measurements from multiple environments with varying multipath characteristics would provide valuable insights into the method's generalizability. The development of standardized benchmarking datasets would further facilitate comparative analysis of different Channel Charting approaches, establishing a common foundation for evaluating new methodologies.

6.1.2 Dissimilarity Matrix Optimization

The current implementation faces challenges with sparse dissimilarity matrices due to the upper bound constraint on moving distances. Future research should address this limitation through several key improvements. Advanced fusion techniques should be developed to better combine TRRS-based moving distance and cosine dissimilarity metrics, potentially incorporating additional complementary measures. Investigation of alternative normalization methods would ensure more consistent distance representation across different metrics. Furthermore, the development of adaptive weighting schemes for metric fusion based on measurement confidence could enhance the reliability of the final dissimilarity matrix.

6.1.3 Deep Learning Architecture Enhancement

The manifold learning phase presents several opportunities for improvement through architectural innovations. Future work should explore and compare alternative deep learning architectures to identify optimal configurations for Channel Charting applications. The development of specialized attention mechanisms could enhance the network's ability to focus on more reliable measurements, potentially improving mapping accuracy. Integration of uncertainty estimation in the mapping process would provide valuable confidence metrics for downstream applications. Additionally, investigation of semi-supervised learning approaches could leverage partially labeled data to improve mapping performance while maintaining the system's self-supervised nature.

6.1.4 Practical Applications

The practical deployment potential of this technology can be enhanced through several key developments. Real-time processing capabilities should be developed to enable dynamic environment mapping, allowing the system to adapt to changing conditions. Integration with existing wireless infrastructure would facilitate seamless deployment in real-world settings, reducing implementation barriers. Research into privacy-preserving techniques would address security concerns in sensitive applications, making the technology more suitable for widespread adoption.

6.2 Conclusion

This research set out to develop a novel approach for Channel Charting by leveraging the Time Reversal Resonating Effect, aiming to overcome the limitations of existing methods that rely on explicit position information or impose restrictive assumptions about user motion. The investigation employed a three-stage methodology: first, implementing TRRS-based moving distance calculation through analysis of CSI measurements; second, constructing and refining a dissimilarity matrix that captures spatial relationships; and third, applying manifold learning techniques for dimensional reduction. The experimental results demonstrated significant achievements, including high accuracy in moving distance estimation (MSE of 0.1691 m, MAE of 0.2932 m) and superior performance in channel chart generation compared to baseline methods, as evidenced by improved Continuity, Trustworthiness, and Kruskal's Stress metrics. These findings indicate that TRRS-based moving distance serves as an effective proxy for spatial relationships in wireless environments, offering a promising solution for privacy-preserving indoor localization without requiring specialized hardware or explicit position labels. The study's primary contribution lies in establishing a theoretical and practical framework that bridges the gap between time-reversal principles and radio environment mapping, while introducing novel techniques for handling trajectory-dependent effects and preserving both local and global spatial relationships. However, several limitations warrant acknowledgment: the current approach faces challenges with sparse dissimilarity matrices, exhibits sensitivity to trajectory patterns in the training data, and requires further validation across diverse environmental conditions. Looking forward, these limitations suggest promising directions for future research, including the development of enhanced fusion techniques for dissimilarity metrics, collection of more diverse datasets, and investigation of advanced deep learning architectures for improved robustness and generalization.

References

[1] Qianqian Zhang and Walid Saad. Semi-supervised learning for channel charting-aided iot localization in millimeter wave networks. In *2021 IEEE Global Communications Conference (GLOBECOM)*, pages 1–6. IEEE, 2021.

[2] Martin Kasparick, Renato LG Cavalcante, Stefan Valentin, S lawomir Stańczak, and Masahiro Yukawa. Kernel-based adaptive online reconstruction of coverage maps with side information. *IEEE Transactions on Vehicular Technology*, 65(7):5461–5473, 2015.

[3] Parham Kazemi, Tushara Ponnada, Hanan Al-Tous, Ying-Chang Liang, and Olav Tirkkonen. Channel charting based beam snr prediction. In *2021 Joint European Conference on Networks and Communications & 6G Summit (EuCNC/6G Summit)*, pages 72–77. IEEE, 2021.

[4] Pulok Tarafder, Chanjun Chun, Arif Ullah, Yonggang Kim, and Wooyeol Choi. Channel estimation in 5g-and-beyond wireless communication: A comprehensive survey. *Electronics*, 14(4):750, 2025.

[5] Ping Zhao, Wuwu Liu, Guanglin Zhang, Zongpeng Li, and Lin Wang. Preserving privacy in wifi localization with plausible dummy locations. *IEEE Transactions on Vehicular Technology*, 69(10):11909–11925, 2020.

[6] Maximilian Stahlke. *Channel Charting assisted Radio Localization: Towards Reliability and Robustness*. PhD thesis, Dissertation, Erlangen, Friedrich-Alexander-Universität Erlangen-Nürnberg . . . .

[7] Moustafa Youssef, Adel Youssef, Chuck Rieger, Udaya Shankar, and Ashok Agrawala. Pinpoint: An asynchronous time-based location determination system. In *Proceedings of the 4th international conference on Mobile systems, applications and services*, pages 165–176, 2006.

[8] Nissanka B Priyantha, Anit Chakraborty, and Hari Balakrishnan. The cricket location-support system. In *Proceedings of the 6th annual international conference on Mobile computing and networking*, pages 32–43, 2000.

[9] Yi Li and Kun Yan. Indoor localization based on radio and sensor measurements. *IEEE Sensors Journal*, 21(22):25090–25097, 2021.

[10] Phillip Stephan, Florian Euchner, and Stephan Ten Brink. Angle-delay profile-based and timestamp-aided dissimilarity metrics for channel charting. *IEEE Transactions on Communications*, 2024.

[11] Zheng Yang, Chenshu Wu, and Yunhao Liu. Locating in fingerprint space: Wireless indoor localization with little human intervention. In *Proceedings of the 18th annual international conference on Mobile computing and networking*, pages 269–280, 2012.

[12] Zheng Yang, Zimu Zhou, and Yunhao Liu. From rssi to csi: Indoor localization via channel response. *ACM Computing Surveys (CSUR)*, 46(2):1–32, 2013.

[13] Christoph Studer, Saïd Medjkouh, Emre Gonultaş, Tom Goldstein, and Olav Tirkkonen. Channel charting: Locating users within the radio environment using channel state information. *IEEE Access*, 6:47682–47698, 2018.

[14] Luc Le Magoarou. Efficient channel charting via phase-insensitive distance computation. *IEEE Wireless Communications Letters*, 10(12):2634–2638, 2021.

[15] Pengzhi Huang, Oscar Castañeda, Emre Gönültaş, Saïd Medjkouh, Olav Tirkkonen, Tom Goldstein, and Christoph Studer. Improving channel charting with representation-constrained autoencoders. In *2019 IEEE 20th International Workshop on Signal Processing Advances in Wireless Communications (SPAWC)*, pages 1–5. IEEE, 2019.

[16] Eric Lei, Oscar Castañeda, Olav Tirkkonen, Tom Goldstein, and Christoph Studer. Siamese neural networks for wireless positioning and channel charting. In *2019 57th Annual Allerton Conference on Communication, Control, and Computing (Allerton)*, pages 200–207. IEEE, 2019.

[17] Florian Euchner, Phillip Stephan, and Stephan Ten Brink. Leveraging the doppler effect for channel charting. In *2024 IEEE 25th International Workshop on Signal Processing Advances in Wireless Communications (SPAWC)*, pages 731–735. IEEE, 2024.

[18] Longhai Zhao, Yunchuan Yang, Qi Xiong, He Wang, Bin Yu, Feifei Sun, and Chengjun Sun. A signature based approach towards global channel charting with ultra low complexity. In *2024 IEEE International Conference on Communications Workshops (ICC Workshops)*, pages 667–672. IEEE, 2024.

[19] Bo Yang, Luyao Guo, Ruijie Guo, Miaomiao Zhao, and Tiantian Zhao. A novel trilateration algorithm for rssi-based indoor localization. *IEEE Sensors Journal*, 20(14):8164–8172, 2020.

[20] Faheem Zafari, Athanasios Gkelias, and Kin K Leung. A survey of indoor localization systems and technologies. *IEEE Communications Surveys & Tutorials*, 21(3):2568–2599, 2019.

[21] Chenshu Wu, Zheng Yang, Yunhao Liu, and Wei Xi. Will: Wireless indoor localization without site survey. *IEEE Transactions on Parallel and Distributed systems*, 24(4):839–848, 2012.

[22] Philipp Bolliger. Redpin-adaptive, zero-configuration indoor localization through user collaboration. In *Proceedings of the first ACM international workshop on Mobile entity localization and tracking in GPS-less environments*, pages 55–60, 2008.

[23] Dragos Niculescu and Badri Nath. Ad hoc positioning system (aps) using aoa. In *IEEE INFOCOM 2003. Twenty-second Annual Joint Conference of the IEEE Computer and Communications Societies (IEEE Cat. No. 03CH37428)*, volume 3, pages 1734–1743. Ieee, 2003.

[24] Feng Qin, Tao Zuo, and Xing Wang. Ccpos: Wifi fingerprint indoor positioning system based on cdae-cnn. *Sensors*, 21(4):1114, 2021.

[25] Jiazhi Ni, Fusang Zhang, Jie Xiong, Qiang Huang, Zhaoxin Chang, Junqi Ma, BinBin Xie, Pengsen Wang, Guangyu Bian, Xin Li, et al. Experience: Pushing indoor localization from laboratory to the wild. In *Proceedings of the 28th Annual International Conference on Mobile Computing And Networking*, pages 147–157, 2022.

[26] Jun-geun Park, Ben Charrow, Dorothy Curtis, Jonathan Battat, Einat Minkov, Jamey Hicks, Seth Teller, and Jonathan Ledlie. Growing an organic indoor location system. In *Proceedings of the 8th international conference on Mobile systems, applications, and services*, pages 271–284, 2010.

[27] Suining He and S-H Gary Chan. Wi-fi fingerprint-based indoor positioning: Recent advances and comparisons. *IEEE Communications Surveys & Tutorials*, 18(1):466–490, 2015.

[28] Hui Zhu, Li Cheng, Xuan Li, and Haiwen Yuan. Neural-network-based localization method for wi-fi fingerprint indoor localization. *Sensors*, 23(15):6992, 2023.

[29] Rashmi Sharan Sinha and Seung-Hoon Hwang. Improved rssi-based data augmentation technique for fingerprint indoor localisation. *Electronics*, 9(5):851, 2020.

[30] Patrick Agostini, Zoran Utkovski, and S lawomir Stańczak. Channel charting: An euclidean distance matrix completion perspective. In *ICASSP 2020-2020 IEEE International Conference on Acoustics, Speech and Signal Processing (ICASSP)*, pages 5010–5014. IEEE, 2020.

[31] Maximilian Stahlke, George Yammine, Tobias Feigl, Bjoern M Eskofier, and Christopher Mutschler. Velocity-based channel charting with spatial distribution map matching. *IEEE Journal of Indoor and Seamless Positioning and Navigation*, 2024.

[32] Chenshu Wu, Feng Zhang, Yusen Fan, and KJ Ray Liu. Rf-based inertial measurement. In *Proceedings of the ACM Special Interest Group on Data Communication*, pages 117–129. 2019.

[33] Geoffroy Lerosey, Julien de Rosny, Arnaud Tourin, Arnaud Derode, Gabriel Montaldo, and Mathias Fink. Time reversal of electromagnetic waves. *Physical review letters*, 92(19):193904, 2004.

[34] Zhung-Han Wu, Yi Han, Yan Chen, and KJ Ray Liu. A time-reversal paradigm for indoor positioning system. *IEEE Transactions on Vehicular Technology*, 64(4):1331–1339, 2015.

[35] Marina Meilă and Hanyu Zhang. Manifold learning: What, how, and why. *Annual Review of Statistics and Its Application*, 11(1):393–417, 2024.

[36] Ian T Jolliffe and Jorge Cadima. Principal component analysis: a review and recent developments. *Philosophical transactions of the royal society A: Mathematical, Physical and Engineering Sciences*, 374(2065):20150202, 2016.

[37] Al Mead. Review of the development of multidimensional scaling methods. *Journal of the Royal Statistical Society: Series D (The Statistician)*, 41(1):27–39, 1992.

[38] Sam T Roweis and Lawrence K Saul. Nonlinear dimensionality reduction by locally linear embedding. *science*, 290(5500):2323–2326, 2000.

[39] Gautam Pai, Ronen Talmon, Alex Bronstein, and Ron Kimmel. Dimal: Deep isometric manifold learning using sparse geodesic sampling. In *2019 IEEE Winter Conference on Applications of Computer Vision (WACV)*, pages 819–828. IEEE, 2019.

[40] Junquan Deng, Saïd Medjkouh, Nicolas Malm, Olav Tirkkonen, and Christoph Studer. Multipoint channel charting for wireless networks. In *2018 52nd Asilomar Conference on Signals, Systems, and Computers*, pages 286–290. IEEE, 2018.

[41] Maximilian Stahlke, George Yammine, Tobias Feigl, Bjoern M Eskofier, and Christopher Mutschler. Indoor localization with robust global channel charting: A time-distance-based approach. *IEEE Transactions on Machine Learning in Communications and Networking*, 1:3–17, 2023.

[42] Paul Ferrand, Alexis Decurninge, Luis G Ordoñez, and Maxime Guillaud. Triplet-based wireless channel charting. In *GLOBECOM 2020-2020 IEEE Global Communications Conference*, pages 1–6. IEEE, 2020.

[43] Brian Rappaport, Emre Gönültaş, Jakob Hoydis, Maximilian Arnold, Pavan Koteshwar Srinath, and Christoph Studer. Improving channel charting using a split triplet loss and an inertial regularizer. In *2021 17th International Symposium on Wireless Communication Systems (ISWCS)*, pages 1–6. IEEE, 2021.

[44] Ilia Karmanov, Farhad G Zanjani, Ishaque Kadampot, Simone Merlin, and Daniel Dijkman. Wicluster: Passive indoor 2d/3d positioning using wifi without precise labels. In *2021 IEEE Global Communications Conference (GLOBECOM)*, pages 1–7. IEEE, 2021.

[45] Florian Euchner, Phillip Stephan, Marc Gauger, Sebastian Dörner, and Stephan Ten Brink. Improving triplet-based channel charting on distributed massive mimo measurements. In *2022 IEEE 23rd International Workshop on Signal Processing Advances in Wireless Communication (SPAWC)*, pages 1–5. IEEE, 2022.

[46] Chenshu Wu, Feng Zhang, Yuqian Hu, and KJ Ray Liu. Gaitway: Monitoring and recognizing gait speed through the walls. *IEEE Transactions on Mobile Computing*, 20(6):2186–2199, 2020.

[47] Sheng Lyu and Chenshu Wu. Ase: Practical acoustic speed estimation beyond doppler via sound diffusion field. *arXiv preprint arXiv:2412.20142*, 2024.

[48] Feng Zhang, Chen Chen, Beibei Wang, Hung-Quoc Lai, Yi Han, and KJ Ray Liu. Wiball: A time-reversal focusing ball method for decimeter-accuracy indoor tracking. *IEEE Internet of Things Journal*, 5(5):4031–4041, 2018.

[49] Florian Euchner, Marc Gauger, Sebastian Dörner, and Stephan ten Brink. A Distributed Massive MIMO Channel Sounder for ”Big CSI Data”-driven Machine Learning. In *WSA 2021; 25th International ITG Workshop on Smart Antennas*, 2021.

[50] Abbas Abolfathi Momtaz, Fereidoon Behnia, Rouhollah Amiri, and Farokh Marvasti. Nlos identification in range-based source localization: Statistical approach. *IEEE Sensors Journal*, 18(9):3745–3751, 2018.

[51] Zhenghua Chen, Qingchang Zhu, and Yeng Chai Soh. Smartphone inertial sensor-based indoor localization and tracking with ibeacon corrections. *IEEE Transactions on Industrial Informatics*, 12(4):1540–1549, 2016.

[52] Kanyanee Phutcharoen, Monchai Chamchoy, and Pichaya Supanakoon. Accuracy study of indoor positioning with bluetooth low energy beacons. In *2020 joint international conference on digital arts, media and technology with ECTI northern section conference on electrical, electronics, computer and telecommunications engineering (ECTI DAMT & NCON)*, pages 24–27. IEEE, 2020.

[53] Vahideh Moghtadaiee and Andrew G Dempster. Indoor location fingerprinting using fm radio signals. *IEEE Transactions on Broadcasting*, 60(2):336–346, 2014.

[54] Jaron Fontaine, Ben Van Herbruggen, Adnan Shahid, Sebastian Kram, Maximilian Stahlke, and Eli De Poorter. Ultra wideband (uwb) localization using active cir-based fingerprinting. *IEEE Communications Letters*, 27(5):1322–1326, 2023.

[55] Liqiong Chang, Jie Xiong, Yu Wang, Xiaojiang Chen, Junhao Hu, and Dingyi Fang. iupdater: Low cost rss fingerprints updating for device-free localization. In *2017 IEEE 37th International Conference on Distributed Computing Systems (ICDCS)*, pages 900–910. IEEE, 2017.

[56] Lionel M Ni, Yunhao Liu, Yiu Cho Lau, and Abhishek P Patil. Landmarc: Indoor location sensing using active rfid. In *Proceedings of the First IEEE International Conference on Pervasive Computing and Communications, 2003.(PerCom 2003).*, pages 407–415. IEEE, 2003.

[57] Shuang Shang and Lixing Wang. Overview of wifi fingerprinting-based indoor positioning. *IET Communications*, 16(7):725–733, 2022.

[58] Paramvir Bahl and Venkata N Padmanabhan. Radar: An in-building rf-based user location and tracking system. In *Proceedings IEEE INFOCOM 2000. Conference on computer communications. Nineteenth annual joint conference of the IEEE computer and communications societies (Cat. No. 00CH37064)*, volume 2, pages 775–784. Ieee, 2000.

[59] Yogita Chapre, Prasant Mohapatra, Sanjay Jha, and Aruna Seneviratne. Received signal strength indicator and its analysis in a typical wlan system (short paper). In *38th Annual IEEE Conference on Local Computer Networks*, pages 304–307. IEEE, 2013.

[60] Xu Feng, Khuong An Nguyen, and Zhiyuan Luo. A survey of deep learning approaches for wifi-based indoor positioning. *Journal of Information and Telecommunication*, 6(2):163–216, 2022.

[61] Ruichen Wang and Dinesh Manocha. Em-gansim: Real-time and accurate em simulation using conditional gans for 3d indoor scenes. *arXiv preprint arXiv:2405.17366*, 2024.

[62] Dorian Pyle. *Data preparation for data mining*. morgan kaufmann, 1999.

[63] Department of Computer Science, HKU. Evacuation Plan Library Building (New Wing) First Floor. The floor plan is provided by the Department of Computer Science, The University of Hong Kong, 2024.

[64] Aditya Arun, Akshaj Bharadwaj, and Roshan Ayyalasomayajula. Wi-fi indoor localization dataset (wild-v2). https://kaggle.com/competitions/wild-v2, 2022. Kaggle.